Cascade sliding mode control implementation in photovoltaic power supply for camping-car applications

Abdelaziz Zaidi* (iD)

University of Kairouan, High Institute of Applied Sciences and Technology, Laboratory of Analysis and Control of Systems (LACS), Tunis 1240, Tunisia, abdelaziz.zaidi@issatkr.u-kairouan.tn

Mohamed Chrigui (iD)

University of Kairouan, High Institute of Applied Sciences and Technology, Laboratory of Analysis and Control of Systems (LACS), Tunis 1240, Tunisia, chriguiimohamed91@gmail.com

Nadia Zanzouri (iD)

University of El Manar, National School of Engineers of Tunis, Laboratory of Analysis and Control of Systems (LACS), Tunis 1240, Tunisia, nadia.zanzouri@enit.rnu.tn

Corresponding Author

Abstract: A cascade proportional integral sliding mode control for a two-stage interleaved boost converter (2IBC) serving as a reliable supplementary power source for camping-car applications is reported. Unlike the active fault-tolerant control approaches used for interleaved boost converters, which require controller reconfiguration, the proposed control scheme is passive fault-tolerant and does not require reconfiguration in the event of a faulty stage. The 2IBC model is analyzed together with the most important parasitic parameters, then, the averaged state-space model is derived to implement the control scheme. The appropriate linear cascade control is determined by using the small-signal equivalent model and improving the robustness and dynamic performance, thereby a proportional integrator controller is replaced by a sliding mode controller. The prototype system uses a signal processor and a low-power solar panel. The control code is generated by a PSIM software and loaded to the via a code composer tool. The experimental results validate the control design and demonstrate the efficiency of the proposed control scheme. In addition, the proposed controller ensures the continuity of service in the event of a faulty stage by verifying the reliability of the power supply.

Keywords: *Boost converter, Camping-car, Cascade sliding mode, Control, Photovoltaic*

1. INTRODUCTION

One question that still awaits an answer today is what will be the best energy source for future cars. While car manufacturers offer some solutions on energy needs of future vehicles, determination of the best option is not a straightforward decision as there are several constraints to consider, including ecological, economic, and technological concerns. Purely electric cars have the advantage of producing zero CO_2 emissions and being low pollution. They also require little maintenance due to the improvements in the field of electric machines. However, recharging the batteries remains a significant challenge in this context. Over 17 million hybrid electric vehicles have been sold worldwide following their introduction in 1997 in the car market. These vehicles are reputed to be environmentally friendly and they offer some advantages in addition to some disadvantages, too. They are designed for short distance trips with frequent stops and starts, and do not allow for fast driving in electric mode. Batteries and their technologies have a significant impact on the reliability of these vehicles. However, electric vehicles (EVs) face with some challenges such as battery health degradation, battery management complexities, appropriate charging strategies and power electronics integration. Therefore, further technical exploration is required to select appropriate battery storage and management system, algorithms, technologies, and controllers [1]. The power supply system of EVs is a multifaceted network involving not only battery cells and modules, but also many other components. If any of these components fails, it could result in a system breakdown [2]. On the one hand, the degradation of the electric battery can have an important effect on fuel consumption, as demonstrated in Ref. [3]. This crucial component increases the weight of the car, resulting in increased fuel consumption at high speeds. For this reason, most car travelers do not consider hybrid or electric cars as ideal for vacations in the present stage.

The integration of renewable energies continues to be a major focus for researchers and engineers, with the goal of incorporating them into our homes and cars. For at least three decades, the hydrogen fuel cell has been a subject of significant interest for scientists and development engineers working for automobile manufacturers as an alternative to the combustion engine. However, the durability of fuel cells is limited, as their performance degrades over time due to aging and fault conditions, as stated in Ref. [4]. Since the invention of photovoltaic cells, various prototypes of solar cars have been designed in universities and industrial environments [5]. These electric cars use batteries that can be recharged by natural light. When natural light is insufficient, the car uses the energy stored in the batteries. Ref. [6] reviews different types of photovoltaic modules, their efficiency, and the challenges associated with integrating them into EVs. It also discusses potential solutions to overcome these challenges and improve the integration of solar power in electric vehicles. In 2014, the Ford C-Max Solar Energy was created as the first real solar car. However, this model is no longer manufactured due to the reduced efficiency of solar panels. It is not a rational idea to rely solely on solar power in cars. Instead, we should consider solar energy as a secondary source to benefit from its free and clean energy while also relieving the powertrain system.

Camping cars are one type of vehicle requiring a reliable and non-polluting source of energy. They represent a mobile living environment that can integrate the daily needs of a small group of people. Therefore, autonomy in electricity is a critical consideration for many camping car owners who wish to travel in complete freedom without needing to connect to charging stations. Typically, a camping car with classic fuel consumption has two batteries: The principal battery, which is used to start the engine, and an auxiliary battery that provides 12 V to power on-board equipment, such as lighting, the water pump, television, and fridge. To produce a 12 V_{dc} power supply from a solar panel, a step-up power converter is necessary if the voltage delivered by the panel is less than 12 V, or step-down in other cases. However, this supply is subject to perturbations, such as parasitic parameters of the converter and variations of the load. Therefore, designing an auxiliary power supply requires a robust control and a reliable structure for the converter.

Proper installation and maintenance practices, including regular cleaning and inspection, are essential to increase the reliability and efficiency of photovoltaic (PV) panels [7]. Technology quality is also critical, as reflection from solar module front glass can cause a 4% optical loss, decreasing module efficiency [8]. To sustainably harness energy from PV sources, it is essential to conduct continuous research to address the weaknesses of certain components, including power converters. The interleaved boost converters (IBC) provide an alternative solution to boost the low voltage output from PV panels. Compared to conventional boost converters, the IBC topology has demonstrated higher reliability, as shown in Ref. [9]. In a different study, Reshma et al., [10] presented a comprehensive review of dc-dc converter topologies employed in PV applications, including PV array configurations, advanced Maximum Power Point Tracking (MPPT) techniques, advanced converters, and comparative analysis of hardware complexity, cost, and efficiency.

The impact of parasitic elements on the modeling of dc-dc power converters cannot be ignored. Even though its effect is mainly observed on energy losses, it can significantly impact the performance of the system. Refs. [11,12] provide an analysis and modeling of dc-dc power converter in non-ideal cases, covering both the continuous conduction mode (CCM) and the discontinuous conduction mode (DCM). The control of power converters is a complex problem with an extensive literature on this subject. Regardless of the approach, the primary aim of the control is to optimize the power of the system and maintain it there despite external disturbances and parameter variations. Consequently, nonlinear controllers have emerged as a promising solution due to the strong nonlinearity of PV panel and power converter.

In Ref. [13], an Incremental Conductance Maximum Power Point Tracking (InC MPPT) algorithm is used to control the duty cycle of an interleaved two-stage boost converter (2IBC) and the circuit of power conditioning connected between the PV array and the load, with the aim of extracting maximum power from the source and introducing it to the load. The estimated overall efficiency of the system is around 95%. Furthermore, in Ref. [14], the IBC is modeled and analyzed using an averaging technique in the state space, and small-signal analysis is performed. The 2IBC is analyzed in CCM and a duty cycle greater than 0.5. In a previous study, Thounthong et al., [15] have proposed a control technique based on flatness theory for multi-stack Proton Exchange Membrane Fuel Cell (PEMFC) with multi-phase converters to ensure the dc bus voltage balance of a dc microgrid in the event of load disturbances. Meanwhile, a nonlinear passivity-based control has been suggested in Ref. [16] to order n interleaved boost converters with power factor correction (PFC). Kamaraj et al., [17] developed a control scheme for a three-stage IBC based on fuzzy proportional integral action to regulate the output voltage of the converter. Experimental verification was conducted, demonstrating the effectiveness of the proposed approach compared to the conventional Proportional and Integral (PI) controller.

Many control methodology, including sliding mode control (SMC), have demonstrated their effectiveness. However, the practical implementation of these methods still poses a constraint requirement to be verified. The SMC is an excellent robust controller that is widely used in various applications such as robotics, motors, actuator control, and PV energy systems [18,19,20]. Due to its high performance and simplicity of implementation, it is used for robust nonlinear control of power converters with a real-time experimental validation [18]. Typically, this control method is consolidated with another method to increase efficiency. For instance, Charaabi et al., [21] demonstrated that PI-SMC provides better performance indicators than sliding mode control or cascaded PI-PI alone.

The control scheme presented here is specifically designed for a two-stage boost converter. Our proposal is to exploit the physical redundancy of the interleaved boost converter to apply passive fault tolerant control, thereby enhancing the reliability of the power supply. To achieve this objective, we consider proportional integral sliding mode control, which has been demonstrated to be effective for conventional boost converters. Passive fault tolerant control (FTC) does not require reconfiguration in the event of a predefined set of faults. It is mentioned in Ref. [22] that passive FTC is indeed classified as a robust control. In contrast, active techniques reconfigure control parameters when a fault is detected [23].

The primary contribution of this paper is the design and implementation of passive fault tolerant cascaded proportional integral sliding mode control to a two-stage boost converter in a solar cell-based extra power supply for camping cars or any vehicle with extra electric load applications. A two-stage boost converter has an inherent advantage in that during normal operation, control signals are shifted by π. In the case of a faulty operation, the converter behaves as a conventional one with only one control signal. However, this is not the case with a three-stage boost converter that is reconfigured to a two-stage converter. In such a scenario, the shift must be adjusted from $2\pi/3$ to π to achieve the same performance as a native two-stage converter. The robustness of our approach against load variations will be demonstrated through experimental results. These results will provide verification of the efficacy of our proposed method.

The article is organized as follows: Initially, a problem formulation is presented in Sec. 2. It is followed by a detailed description of the design of the 12 V_{dc} extra power supply in Sec. 3. Besides, information on the control design and implementation with the experimental tests are presented in Sec. 4. Consequently, the final section is devoted to conclusions and future perspectives.

2. PROBLEM FORMULATION

In car applications, the power source with 12 V_{dc} serves for multiple purposes, including starting the engine, powering devices such as cigarette lighters, mp3 and mp4 players, and others. While fossil fuel cars, hybrid, and electric cars have dc power sources in varying ranges, 12 V_{dc} is the most common voltage value required, especially in standardized cars. An auxiliary 12 V_{dc} clean power source is essential and can alleviate the burden on the primary battery. PV battery sources provide a viable alternative to meet this need. The presence of flexible heavy solar panels makes it possible to implement such power supplies on the roof of small or camping cars (as shown in Fig. 1).
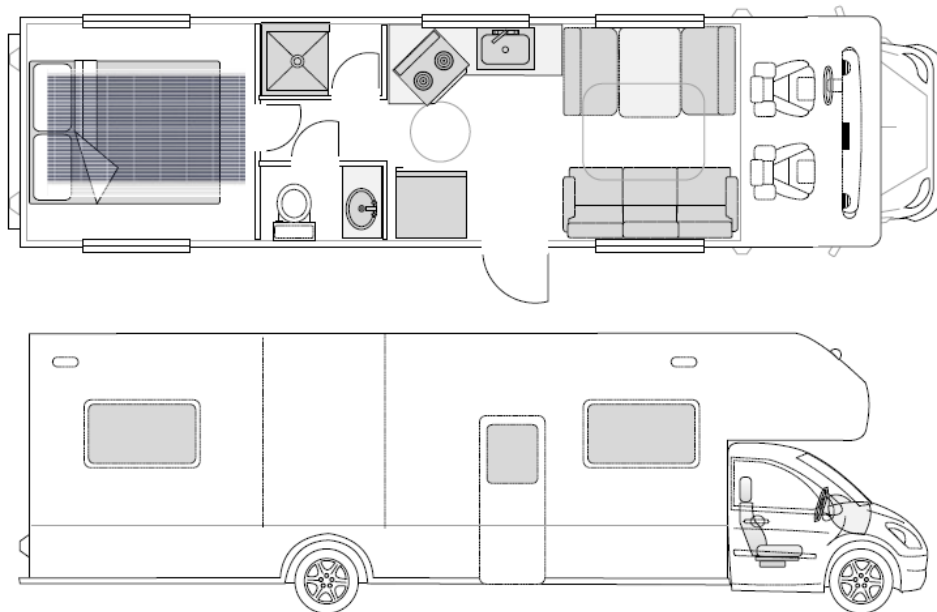

Figure 1. Indication of the placement of a flexible solar panel on a camping car roof.

Generally, the connection of a solar panel with a 12 V_{dc} auxiliary battery is performed according to the schematic of Fig. 2.
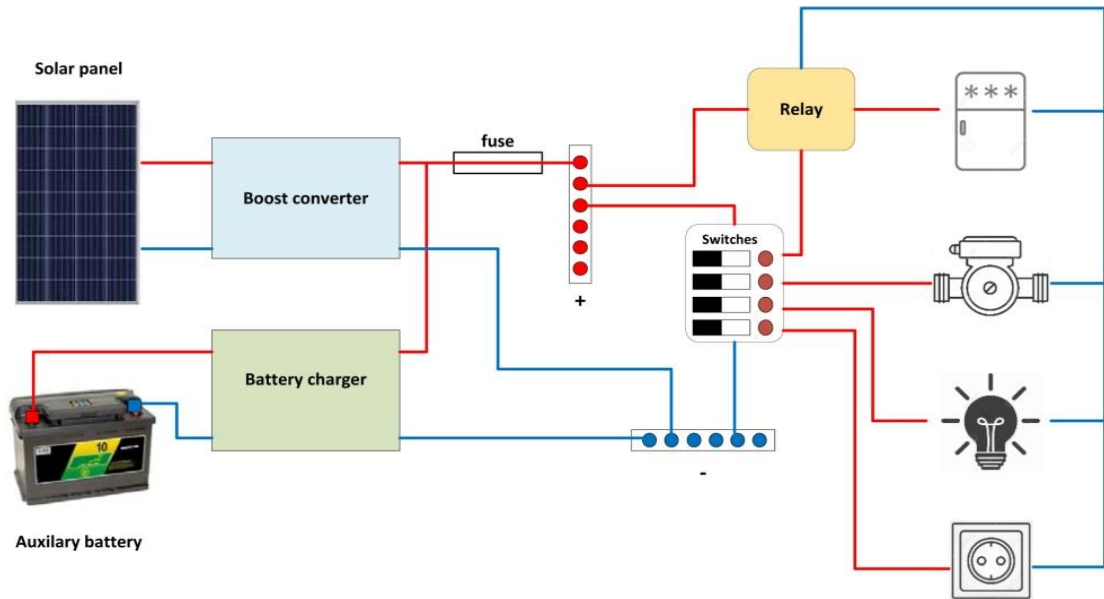
Figure 2. Connection of a sample PV panel with a camping car installation.

This paper presents the design of a low-cost renewable energy source using discrete components for a boost converter. The need for boost converters is due to the low voltage delivered from a PV panel. In Ref. [9], it was demonstrated that three-stage boost converters are more reliable than conventional ones. However, increasing the number of stages could make implementation difficult since all stages must be controlled with signals shifted by the same value.

The objective of this work is to design an auxiliary 12 V_{dc} power supply based on a 6 V & 30 W PV panel, with the retained structure of the converter being two-stage. The primary requirements for such a realization are simplicity, efficiency, and reliability.

3. DESIGN OF THE 12 Vdc POWER SUPPLY

3.1. The Functional Diagram of the Extra Power Supply

The functional diagram of the extra power supply is illustrated in Fig. 3. The choice of interleaved boost converter is based on reliability requirement of the dc power source. In the context of the present paper, it is discussed only the stand-alone power supply and the connection with a 12 V_{dc} battery, for charging purpose, is not evoked.
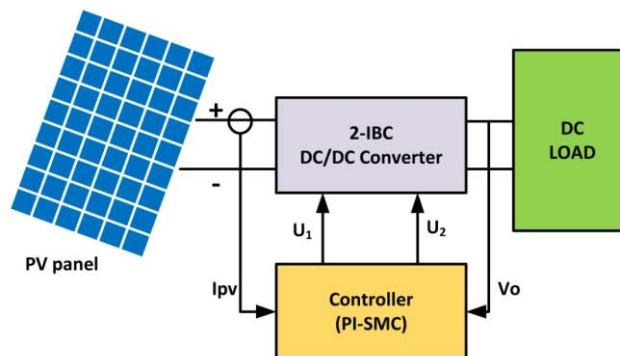

Figure 3. Functional diagram of control approach.

3.2. Interleaved Boost Converters

The applications of interleaved boost converters (IBC) are diverse. Primarily, the purpose of these power converter structures is to address the rise of multisource power systems connected to dc grids such as fuel cells, PV cells, ultra-capacitors, and batteries. Additionally, IBCs aim to enhance the reliability of the dc/dc power converter in the event of fault tolerant control strategies. Photovoltaic cells require boost converters due to the low voltage provided. In a recent study [24], a novel non-isolated dc-dc converter topology was proposed for PV applications. The proposed converter utilizes an IBC to minimize input current ripple. Instead of conventional inductors, the converter employs coupled ones to provide benefits such as high efficiency and reduced switching loss. Consequently, this converter is an excellent choice for stepping up the voltage from the PV source and connecting it to a common 380 V DC bus of a microgrid, making it a noteworthy solution.

In [25], a new approach was presented, suggesting an interleaved boost converter (IBC) as an interface between the photovoltaic (PV) module and a common DC link. This approach demonstrates the converter's effectiveness and reliability in reducing the ripples of PV current, all without using bulky input inductors or increasing the switching frequency. Another proposed solution by Jung, et al., [26] is the interleaved soft switching boost converter (ISSBC) for PV power-generation systems. This topology enhances the converter and PV power conditioning system (PVPCS) efficiency and reduces switching losses by adopting a resonant soft-switching method. With these features, ISSBC represents a promising solution for the improvement of the efficiency of the PVPCS.

Reatti, et al., [12] presented nonlinear models of buck and boost converters, under both ideal (without parasitic parameters) and non-ideal conditions, operating in continuous conduction mode (CCM). Ref. [11] compared two modeling techniques, small-signal and large-signal, for DC-DC converters in discontinuous conduction mode (DCM). This comparison demonstrated that the small-signal equivalent circuit enables a quick and precise frequency domain analysis. Refs. [27-28] studied an improved two-stage boost converter with a coupled inductor in CCM and DCM. They found that the coupling effects on the circuit statuses are independent of the converter load. The converter's operation modes were analyzed, and boundary conditions were derived. In another study [29], the averaged state space technique was utilized to analyze a Multiphase Interleaved Converter. The study derived steady-state and small-signal models for an N-phase interleaved converter and applied their analysis on a 2IBC. Fig. 4 illustrates an N-phase interleaved boost converter.
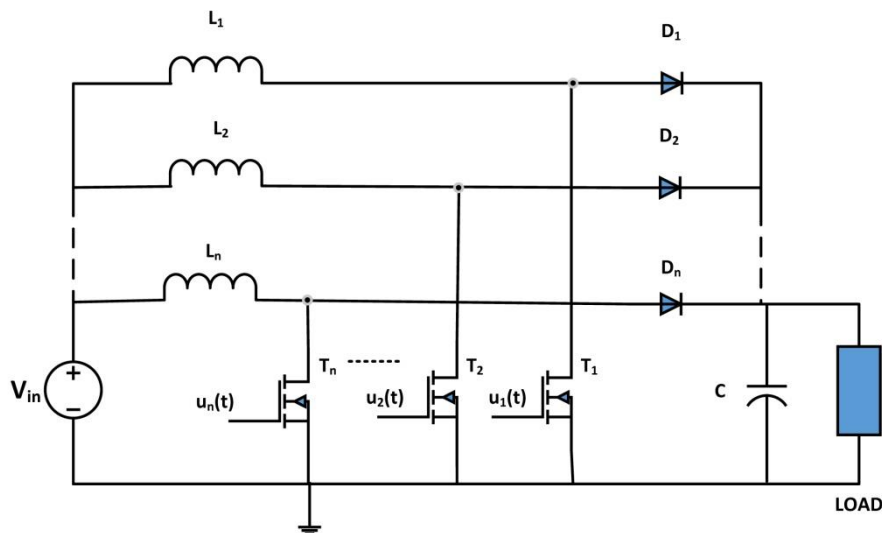

Figure 4. Interleaved Boost converter with N-phase.

Among the advantages of choosing the multi-phase boost converter, one can cite their redundant architectures; if a fault appears on one phase, the other phases can be used as compensation systems,

thereby avoiding a power interruption of energy. Logic signals to all gates are equally phase shifted according to the following equation:

$$Phase\ shift = \frac{2\pi}{N} \tag{1}$$

where N designates the number of converter stages. The averaged model of the interleaved N-stage boost converter is written as,

$$\begin{cases} \dot{x} = Ax + Bv_{in} \\ \quad y = Cx \end{cases} \tag{2}$$

where the state vector is,

$$x = \begin{pmatrix} x_1 \\ x_2 \\ \vdots \\ x_{n-1} \\ x_n \end{pmatrix} = \begin{pmatrix} i_{L1} \\ i_{L2} \\ \vdots \\ i_{Ln} \\ v_c \end{pmatrix}$$

Knowing that a power converter belongs to the class of switching systems, the matrix and vector parameters A, B and C can be determined as

$$A = \sum_{i=1}^{N} d_i A_i \tag{3}$$

$$B = \sum_{i=1}^{N} d_i B_i \tag{4}$$

$$C = \sum_{i=1}^{N} d_i C_i \tag{5}$$

This is based on the assumption that all switching stages carry the same average current and operate at the same ratio cyclically in a switching cycle.

3.3. The Two-Stage Boost Converter

Based on Eq. (1), a two-stage interleaved boost converter (2IBC) requires logic pulse-width modulated (PWM) control signals u_1 and u_2 for the two transistors with a phase shift of π. Depending on the range of the duty cycle, the operation of the 2IBC converter is divided into three cases: $0.5 < d < 1$, $0 < d < 0.5$, and $d = 0.5$. To further analyze the dynamic behavior of 2IBC, mathematical modeling is required. The state-space averaging technique is commonly used in the modeling of power converters. The state variables are the inductance currents (i_1, i_2) and output capacitor voltage (v_c). Circuit analysis for each mode of operation is performed by averaging the product with the duty cycle. The state space model can be written as,

$$\begin{cases} \dot{x} = Ax + Bv_{in} \\ \quad y = Cx \end{cases} \tag{6}$$

The state vector is,

$$x = \begin{pmatrix} i_1 \\ i_2 \\ v_c \end{pmatrix} \qquad (7)$$

The duty cycle d is in [0,1]. The choice of it depends on how is the percentage of the voltage increase in the output of the power converter. The static formula is

$$V_o = \frac{V_{in}}{1-d} \qquad (8)$$

To deduce the dynamic behavior of the converter, one must choose one of the three cases: $0.5 < d < 1$, $0 < d < 0.5$, and $d = 0.5$. The analysis is made with the same reasoning. In the case study of the present paper, d should be equal to 0.5 because the implementation objective is to double the 6VDC delivered by the solar cell. Therefore, there will be two operating intervals as illustrated in Fig. 5. The two operating intervals are: $d_1 \rightarrow T_1$ ON and T_2 OFF; $d_2 \rightarrow T_1$ OFF and T_2 ON. This analysis is made with some assumptions:

- *The switches in the converter are assumed to be ideal.*
- *The converter is operating in the continuous conduction mode.*
- *The converter is assumed to have reached steady-state operation, meaning that all voltages and currents have settled to constant values.*
- *Parasitic elements of inductances and capacitors are taken into account.*
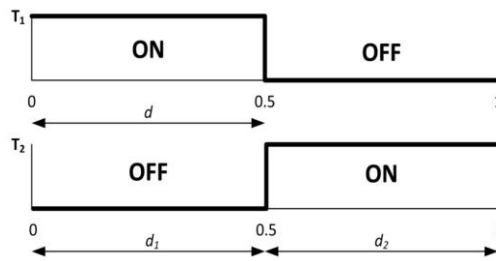- *The input voltage is assumed to be constant over the switching cycle.*

Figure 5. Two operating intervals in the case d = 0.5.

Interval d_1:

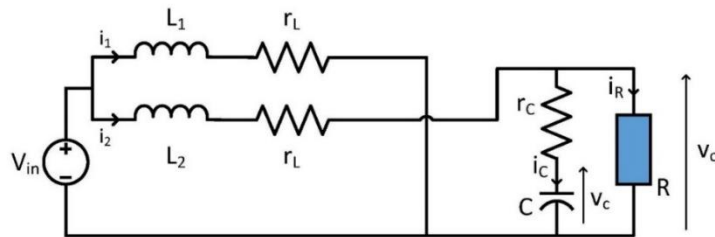From Fig. 6, switch T_1 is open and T_2 is closed.

Figure 6. Equivalent electrical circuit of the 2IBC in interval d1.

According to Fig. 6, the mesh law gives the following equations,

$$\begin{cases} v_{in} = r_1 i_1 + L \dfrac{di_1}{dt} \\ v_{in} = r_L i_2 + L \dfrac{di_2}{dt} + v_o \\ v_c = v_o - r_c i_c \end{cases} \qquad (9)$$

where r_L and r_c are respectively the parasitic resistances of the inductance and the capacitor and $L_1 = L_2 = L$.

Knowing that $i_2 = i_c + i_R = C\dfrac{dv_c}{dt} + \dfrac{v_o}{R}$, the following equation can be written,

$$v_{in} = r_L i_2 + L\frac{di_2}{dt} + v_c + r_c C\frac{dv_c}{dt} \tag{10}$$

On the other hand, we have $v_o = Ri_R = R(i_2 - i_c) = Ri_2 - RC\dfrac{dv_c}{dt}$, which means,

$$v_{in} = r_L i_2 + L\frac{di_2}{dt} + Ri_2 - RC\frac{dv_c}{dt} \tag{11}$$

Equalizing Eqs. (10) and (11) yields to,

$$\frac{dv_c}{dt} = \frac{R}{(R + r_c)C} i_2 - \frac{1}{(R + r_c)C} v_c \tag{12}$$

Replacing Eq. (12) in Eq. (10) gives,

$$\frac{di_2}{dt} = -\frac{2R^2 + (r_c + r_L)R + r_c r_L}{(R + r_c)L} i_2 + \frac{R}{(R + r_c)L} v_c + \frac{v_{in}}{L} \tag{13}$$

As a result, the differential equivalent system will be,

$$\begin{cases} \dfrac{di_1}{dt} = -\dfrac{r_L}{L} i_1 + \dfrac{v_{in}}{L} \\[2mm] \dfrac{di_2}{dt} = -\dfrac{2R^2 + (r_c + r_L)R + r_c r_L}{(R + r_c)L} i_2 + \dfrac{R}{(R + r_c)L} v_c + \dfrac{v_{in}}{L} \\[2mm] \dfrac{dv_c}{dt} = \dfrac{R}{(R + r_c)C} i_2 - \dfrac{1}{(R + r_c)C} v_c \end{cases} \tag{14}$$

The output voltage v_o is expressed as,

$$v_o = \frac{r_c R}{R + r_c} i_2 + \frac{R}{R + r_c} v_c \tag{15}$$

From Eqs. (14) and (15), the state space model is given by,

$$A_1 = \begin{pmatrix} -\dfrac{r_L}{L} & 0 & 0 \\[3mm] 0 & -\dfrac{2R^2 + (r_c + r_L)R + r_c r_L}{(R + r_c)L} & \dfrac{R}{(R + r_c)L} \\[3mm] 0 & \dfrac{R}{(R + r_c)C} & -\dfrac{1}{(R + r_c)C} \end{pmatrix} \tag{16}$$

$$B_1 = \begin{pmatrix} \frac{1}{L} \\ \frac{1}{L} \\ 0 \end{pmatrix}; \quad C_1 = \begin{pmatrix} 0 & \frac{r_c R}{R + r_c} & \frac{R}{R + r_c} \end{pmatrix} \tag{17}$$

nterval d_2:

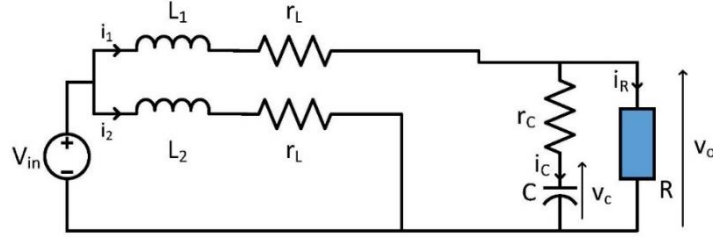Switch T_1 is closed and T_2 is open as shown in Fig. 7.

Figure 7. Equivalent electrical circuit of the 2IBC in interval d2.

According to circuit current law, the following equations can be deduced as follows:

$$\begin{cases} \dfrac{di_1}{dt} = -\dfrac{2R^2 + (r_{c+}r_L)R + r_c r_L}{(R + r_c)L} i_1 + \dfrac{R}{(R + r_c)L} v_c + \dfrac{v_{in}}{L} \\ \dfrac{di_2}{dt} = -\dfrac{r_L}{L} i_2 + \dfrac{v_{in}}{L} \\ \dfrac{dv_c}{dt} = \dfrac{R}{(R + r_c)C} i_1 - \dfrac{1}{(R + r_c)C} v_c \end{cases} \tag{18}$$

and

$$v_o = \frac{r_c R}{R + r_c} i_1 + \frac{R}{R + r_c} v_c \tag{19}$$

From Eqs. (18) and (19), the state space model is given by,

$$A_2 = \begin{pmatrix} -\dfrac{2R^2 + (r_{c+}r_L)R + r_c r_L}{(R + r_c)L} & 0 & \dfrac{R}{(R + r_c)L} \\ 0 & -\dfrac{r_L}{L} & 0 \\ \dfrac{R}{(R + r_c)C} & 0 & -\dfrac{1}{(R + r_c)C} \end{pmatrix} \tag{20}$$

$$B_2 = \begin{pmatrix} \frac{1}{L} \\ \frac{1}{L} \\ 0 \end{pmatrix}; \quad C_2 = \begin{pmatrix} \frac{r_c R}{R + r_c} & 0 & \frac{R}{R + r_c} \end{pmatrix} \tag{21}$$

According to Fig. 5,

$$d_1 = d_2 = d \tag{22}$$

Here, one could write,

$$A = d(A_1 + A_2)$$
$$B = d(B_1 + B_2)$$
$$C = d(C_1 + C_2)$$

By supposing $r_L\ r_c << R(r_L + r_c)$, the matrices A, B, C will be the following

$$A = \begin{pmatrix} -d\left(\dfrac{r_L}{L} + \dfrac{2R^2 + R(r_L + r_c)}{(R + r_c)L}\right) & 0 & \dfrac{dR}{(R + r_c)L} \\[4mm] 0 & -d\left(\dfrac{r_L}{L} + \dfrac{2R^2 + R(r_L + r_c)}{(R + r_c)L}\right) & \dfrac{dR}{(R + r_c)L} \\[4mm] \dfrac{dR}{(R + r_c)C} & \dfrac{dR}{(R + r_c)C} & -\dfrac{2d}{(R + r_c)C} \end{pmatrix} \tag{23}$$

$$B = \begin{pmatrix} \dfrac{2d}{L} \\[3mm] \dfrac{2d}{L} \\[3mm] 0 \end{pmatrix}; \quad C = \left(\dfrac{dRr_c}{R + r_c} \quad \dfrac{dRr_c}{R + r_c} \quad \dfrac{2dR}{R + r_c}\right) \tag{24}$$

Assuming the new simplifying variable definition,

$$\begin{cases} \dfrac{r_L}{L} + \dfrac{2R^2 + R(r_L + r_c)}{(R + r_c)L} = f \\[3mm] \dfrac{R}{(R + r_c)L} = g \\[3mm] \dfrac{1}{(R + r_c)C} = h \end{cases} : \begin{cases} \dfrac{R}{(R + r_c)C} = k \\[3mm] \dfrac{Rr_c}{(R + r_c)} = w \\[3mm] \dfrac{R}{R + r_c} = z \end{cases}$$

The matrices A, B, C will be,

$$A = \begin{pmatrix} -df & 0 & dg \\ 0 & -df & dg \\ dk & dk & -2dh \end{pmatrix} \tag{25}$$

$$B = \begin{pmatrix} \dfrac{2d}{L} \\[3mm] \dfrac{2d}{L} \\[3mm] 0 \end{pmatrix}; \quad C = (dw \quad dw \quad 2dz) \tag{26}$$

The small signals analysis allows us to deduce the linear model, therefore we assume: $x = X + \tilde{x}$. The signals are divided into a continuous signal (X) plus a low amplitude signal ($\tilde{x}$): $i = I + \tilde{\imath}$; $d = D + \tilde{d}$ and $v_c = V_C + \tilde{v}_c$. These variables should be replaced in the equivalent state space model. Thereafter, static values and signals from second order should be neglected,

$$\begin{cases} \dfrac{d\tilde{\imath}_1}{dt} = -Df\tilde{\imath}_1 + Dg\tilde{v}_c - \tilde{d}\left(fI_1 - gV_C - \dfrac{2}{L}v_{in}\right) \\[2mm] \dfrac{d\tilde{\imath}_2}{dt} = -Df\tilde{\imath}_2 + Dg\tilde{v}_c - \tilde{d}\left(fI_2 - gV_C - \dfrac{2}{L}v_{in}\right) \\[2mm] \dfrac{d\tilde{v}_c}{dt} = Dk\tilde{\imath}_1 + Dk\tilde{\imath}_2 - 2Dh\tilde{v}_c + \tilde{d}((I_1 + I_2)k - 2hV_C) \end{cases} \qquad (27)$$

Supposing that,

$$\begin{cases} f\,I_1 - gV_C - \dfrac{2}{L}v_{in} = \alpha \\[2mm] f\,I_2 - gV_C - \dfrac{2}{L}v_{in} = \beta \\[2mm] (I_1 + I_2)k - 2hV_C = \gamma \end{cases}$$

One can write,

$$\begin{cases} \dfrac{d\tilde{\imath}_1}{dt} = -Df\tilde{\imath}_1 + Dg\tilde{v}_c - \tilde{d}\alpha \\[2mm] \dfrac{d\tilde{\imath}_2}{dt} = -Df\tilde{\imath}_2 + Dg\tilde{v}_c - \tilde{d}\beta \\[2mm] \dfrac{d\tilde{v}_c}{dt} = Dk\tilde{\imath}_1 + Dk\tilde{\imath}_2 - 2Dh\tilde{v}_c + \gamma\tilde{d} \end{cases} \qquad (28)$$

Since two phases are identical and the control signals are shifted by π, the small signal currents should cancel each one the other to reduce the total current ripple. So, one can assume: $\tilde{\imath}_1 = -\tilde{\imath}_2 = \tilde{\imath}$, $I_1 = I_2 = I$ ⇒ α = β, which leads to

$$\begin{cases} \dfrac{d\tilde{\imath}}{dt} = -Df\tilde{\imath} + Dg\tilde{v}_c - \alpha\tilde{d} \\[4mm] \dfrac{d\tilde{v}_c}{dt} = -2Dh\tilde{v}_c + \gamma\tilde{d} \end{cases} \qquad (29)$$

Applying the Laplace transformation of,

$$\begin{cases} s\tilde{\imath}(s) = -Df\tilde{\imath}(s) + Dg\tilde{v}_c(s) - \alpha\tilde{d}(s) \\[2mm] s\tilde{v}_c(s) = -2Dh\tilde{v}_c(s) + \gamma\tilde{d}(s) \end{cases} \qquad (30)$$

After some transformations, it can be deduced,

$$\frac{\tilde{v}_c(s)}{\tilde{d}(s)} = \frac{\gamma}{s + 2Dh} \qquad (31)$$

Due to the low value of the parasitic resistor of the capacitor and for a simplification reason, the output voltage v_o of the 2IBC will be approximated to v_c. Finally, the following transfer functions can be determined

$$G_1(s) = \frac{\tilde{\imath}(s)}{\tilde{d}(s)} = \frac{-\alpha s + Dg\gamma - 2\alpha Dh}{s^2 + D(2h + f)s + 2D^2 fh} \qquad (32)$$

and

$$G_2(s) = \frac{\tilde{v}_o(s)}{\tilde{\imath}(s)} = \frac{\gamma s + Dh\gamma}{-\alpha s + Dg\gamma - 2\alpha Dh} \qquad (33)$$

Knowing that this interleaved boost converter will be associated to a solar panel, the control strategy should by hybrid to increase the efficiency, robustness and performance of the designed renewable energy power source. In the following paragraph, this will be discussed and the final control scheme will be derived.

3.4. The Control Problem

The control of renewable energy sources is a significant research area that has gained attention in recent years. In Ref. [30], Bougrine, et al., developed a hybrid control approach for a two-stage boost converter dedicated to renewable energies and automotive applications, which includes a real-time load estimation using an algebraic approach for the hybrid controller online setting. Another approach used the passivity of the incremental model of the same converter structure with a PI action as a control strategy in [31]. To address performance degradation and system instability resulting from the interactions between individually designed power converters, Liangcai, et al., proposed a new control strategy integrating Active Disturbance Rejection Control (ADRC) and flatness control [32]. In Ref. [14], an analog Proportional Integral Derivative (PID) controller designed based on converter parameters, including parasitic ones, was simulated in open-loop and closed-loop. According to [21-33], cascade control of boost converters is an efficient strategy, and the selected control scheme in this paper will be based on this concept. The desired performance is robustness against not only parasitic parameters but also input and load perturbations, while practical implementation simplicity is also a crucial factor to consider.

3.4.1. Cascaded proportional integral control

The proportional and integral (PI) controller is widely used in industry. It is a linear control approach that requires good knowledge of the system and fine tuning in order to achieve the desired performance. Due to the duality of variables in a DC/DC power converter, the controller should be able to adjust two kinds of variables: inductance current and capacitor output voltage. This is why cascade control could be a natural solution especially when suitable sensors are available.
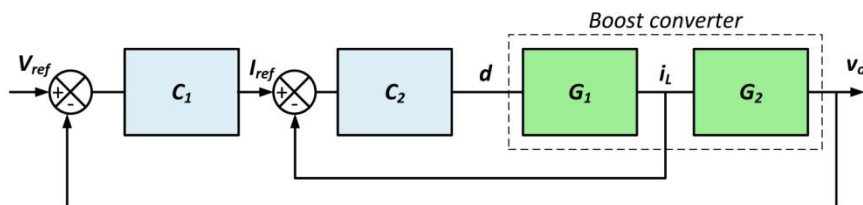

Figure 8. Cascade PI-PI control of the boost converter.

Table 1. The 2IBC technical parameters

Parameter	Value
Input voltage V_{in}	6v
Output voltage V_o	12v
Inductance L_1, L_2	300µH
Output capacitor C_1	47µF
Input capacitor C_2	1000µF
Static duty cycle D	0.5
Load resistor R	50Ω
Transistor parasitic resistor r_{ON}	0.16Ω
Inductance parasitic resistor r_L	1.1Ω
Output capacitor parasitic resistor r_C	2.1Ω
Switching frequency F_s	10KHz

The cascade control structure of a boost converter is portrayed in Fig. 8. The same scheme is used for 2IBC with two control signals shifted by π. The transfer functions G_1 and G_2 are defined by,

$$G_1(p) = \frac{\tilde{\iota}(p)}{\tilde{d}(p)}; \quad G_2(p) = \frac{\tilde{v}_o(p)}{\tilde{\iota}(p)}$$

The parameters of the 2IBC are given in Table 1.

By using equations (32) and (33), the numerical values of $G_1(s)$ and $G_2(s)$ will be

$$G_1(s) = \frac{\tilde{\iota}(s)}{\tilde{d}(s)} = \frac{-8.1836 \times 10^4 s - 1.7744 \times 10^7}{s^2 + 1.6731 \times 10^5 s + 6.8159 \times 10^7}$$

$$G_2(s) = \frac{\tilde{v}_o(s)}{\tilde{\iota}(s)} = \frac{9.8011s + 2.0013 \times 10^3}{-81.836s - 1.7744 \times 10^4}$$

$C_1(s)$ and $C_2(s)$ are the PI controllers, with

$$C_i(s) = K_{Pi} + \frac{K_{Ii}}{s}$$

K_{Pi} and K_{Ii} are respectively the proportional and the integral gains of the controllers. C_1 performs the pursuit of the reference voltage (external loop) and C_2 is dedicated for current regulation (internal loop). C_1 and C_2 will be designed according the following equations

$$\begin{cases} C_1(s) = K_{P1} + \dfrac{K_{I1}}{s} \\ C_2(s) = K_{P2} + \dfrac{K_{I2}}{s} \end{cases}$$

The simulation is done using the SISOTOOL of Matlab software. However, the suitable parameters of the PI controllers are,

$$\begin{cases} K_{p1} = 0.0001 \\ K_{I1} = 5195.2 \\ K_{p2} = 0.9421 \\ K_{I2} = 113.51 \end{cases}$$

Fig. 9 displays the desired step response of the PI-PI cascade control for the 2IBC, exhibiting zero static error, a 21.7% overshoot at 0.015 seconds, and a 5% response time of 0.031 seconds. The performance of this controller is evident from this graph and will be beneficial for future use. However, since the input source will not be constant and disturbances affecting the camping-car load are possible, applying the PI-PI cascade control with the solar panel alone may not achieve the desired control objectives. As previously mentioned, a hybrid approach employing a robust nonlinear control method would be more suitable for such constraints.
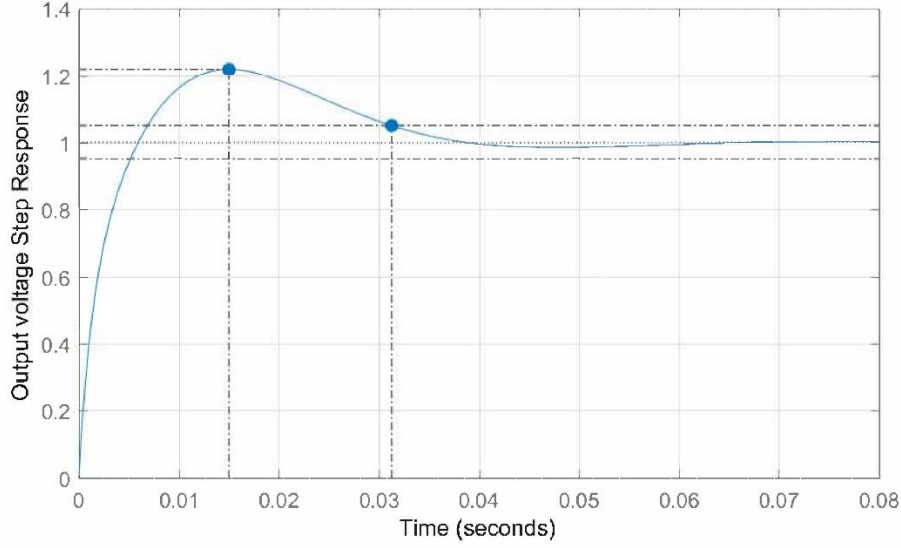
Figure 9. The desired output Step response of cascade PI-PI control of the 2IBC.

3.4.2. Proportional integral sliding mode control

The averaged state space model of the 2IBC is deduced by replacing the ON-OFF control signal with a continuous one which is u ∈ [0,1]. The technique of averaging is widely used because the switching frequency F_s of the PWM signals is higher than the high dynamic frequency of the system. The equivalent model of the converter will be bilinear with the form,

$$\dot{x} = f(x) + g(x)u \tag{34}$$

where $u \in \mathbb{R}^n$ and $x \in \mathbb{R}^m$ are respectively the control input vector and the averaged system state.

The SMC is a nonlinear control which has been proposed firstly for the control of variable structure systems [34]. The principal advantage of SMC is that it guarantees stability and robustness against parameter uncertainties and external load disturbances [35]. Considering a nonlinear system given by Eq. (34). The general design of the control can be performed in two steps: The convergence towards the manifold then sliding on it to achieve the origin. The construction of the manifold is the first step. The general form is proposed by Ref. [36] as follows:

$$sigma(x,t) = \left(\frac{d}{dt} + \lambda\right)^{r-1} \tilde{x}, \tag{35}$$

with $\tilde{x} = x - x_d$ is the error between the controlled variable and its reference, λ is a positive constant and r is the relative degree. In the sliding mode control, two conditions have to be satisfied σ(x) = 0 and $\dot{\sigma}(x)$ = 0. The second step is to determine the control law. Generally, the variable structure sliding mode control law is defined by

$$u = u_{eq} + \Delta u \tag{36}$$

The first term u_{eq} is continuous; it corresponds to the ideal sliding regime. Δu is a commutation term in the form of $(-k.\,\mathrm{sgn}(\sigma))$ with k a constant gain. This term lets the equilibrium point close to the sliding manifold.

u_{eq} can be determined by satisfaction of the invariance conditions,

$$\dot{\sigma}(x) = \frac{\partial \sigma}{\partial x}(f(x) + g(x)u_{eq})\big|_{\sigma=0} = 0$$

$$\Rightarrow L_f\sigma(x) + [L_g\sigma(x)]u_{eq}\big|_{\sigma=0} = 0$$

(37)

where $L_f\sigma(x) = \sum_{i=1}^{n} \frac{\partial \sigma}{\partial x_i} f_i(x)$. Then the expression of u_{eq} will be

$$u_{eq}(x) = -\frac{L_f\sigma(x)}{L_g\sigma(x)}\big|_{\sigma=0}$$

(38)

In the context of controlling the 2IBC, the sliding manifold in the case of pure SMC can be simply chosen to be

$$\text{sigma}(x) = \lambda_1(x_2 - x_{2d}) + \lambda_2(x_1 - x_{1d}),$$

(39)

where x_{2d} and x_{1d} are respectively the reference values of output voltage and the input current and (λ_1, λ_2) are the parameters of the control. The reference of the input current is defined by

$$x_{1d} = I_L = I_{L1} + I_{L2} = \frac{x_{2d}^2}{RV_{in}} = \frac{V_C^2}{RV_{in}}.$$

(40)

Due to the fact that boost converters are minimum phase systems, the control of only the output voltage may cause internal instability. When the sliding manifold depends on both current and voltage references, the chattering phenomena will be obvious and the result is poor [21].

The design of SMC in the current loop does not need to take into account parasitic parameters. Moreover, $f(x)$ and $g(x)$ can be chosen to be equal to the expressions of the equivalent input to output conventional boost converter. This can be performed by equalizing the energy stocked in the inductors [9]. Thereafter, this concept will be verified by simulation and experimental results. Cascaded PI-SMC consists of replacing the inner PI controller (block C_2) by a sliding mode controller. The sliding manifold will be based only on the inductance current $\big(\text{sigma}(x) = \lambda(x_1 - x_{1d})\big)$. This will give the following performances compared to SMC approach presented in the beginning of the paragraph:

- *Reducing chattering,*
- *More robust,*
- *Fast transient response under load resistance and input voltage variations,*
- *Steady state error is less.*

4. IMPLEMENTATION AND EXPERIMENTAL RESULTS

4.1. The Prototype

The simulation of the proposed models of the 2IBC converter and the control scheme is essentially based on the PSIM tool (https://powersimtech.com/). Subsequently, the continuous domain simulation schemes will be translated into the discrete domain for implementation in the digital signal processor (DSP) TI F28335. The control program is generated by the software according the discrete translation of the continuous model with inserting the Pulse Width Modulation (PWM) and analog to digital converter (ADC) DSP modules and the hardware configuration. The practical assembly of the project is given in Fig. 10.
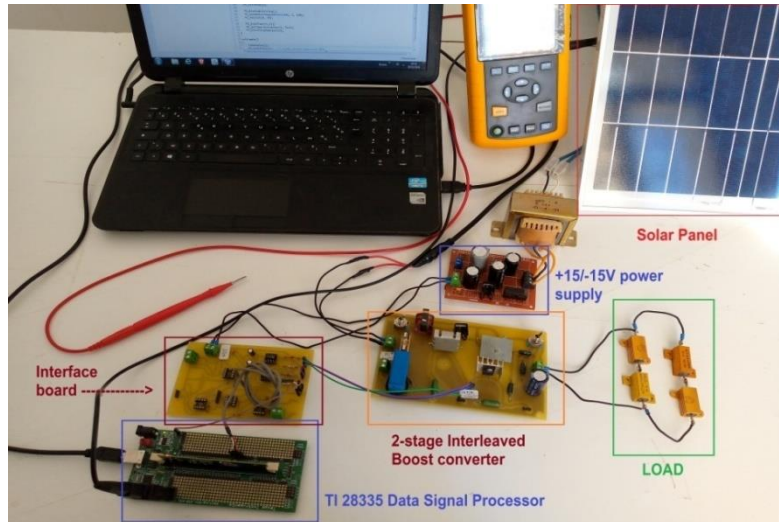
Figure 10. The experimental prototype.

The TMDSDOCK28335 is a C2000 experiment kit from Texas Instruments. The most important technical characteristics are:

- *Control board based on TMS320F28335 MCU (32-bit DSP).*
- *Frequency up to 150 MHz (6.67 ns cycle time).*
- *9 timers 32-bit (6 for ePWMs).*
- *12-bit ADC, 16 channels – 80 ns conversion time.*
- *USB emulation on board or possibility to use an external JTAG emulator.*
- *18 PWM outputs.*
- *Development support is Code Composer Studio (https://www.ti.com/tool/CCSTUDIO) which includes ANSI C/C++ compiler/assembler/linker.*

The possible applications are varied: motor control, alternative energy, power management, lighting, automotive, etc. Table 2 gives the technical characteristics of the solar panel used in experiments. We recall that the parameters of the 2IBC are shown in Table 1.

Table 2. Technical characteristics of the solar panel

Parameter	Value
Maximum power P_{max}	30W
Maximum power voltage V_{mp}	6V
Maximum power current I_{mp}	5A
Open circuit voltage V_{OC}	7.2V
Short circuit current I_{SC}	6A
Size	350×530×17mm

4.2. Implementation of the Control Algorithm

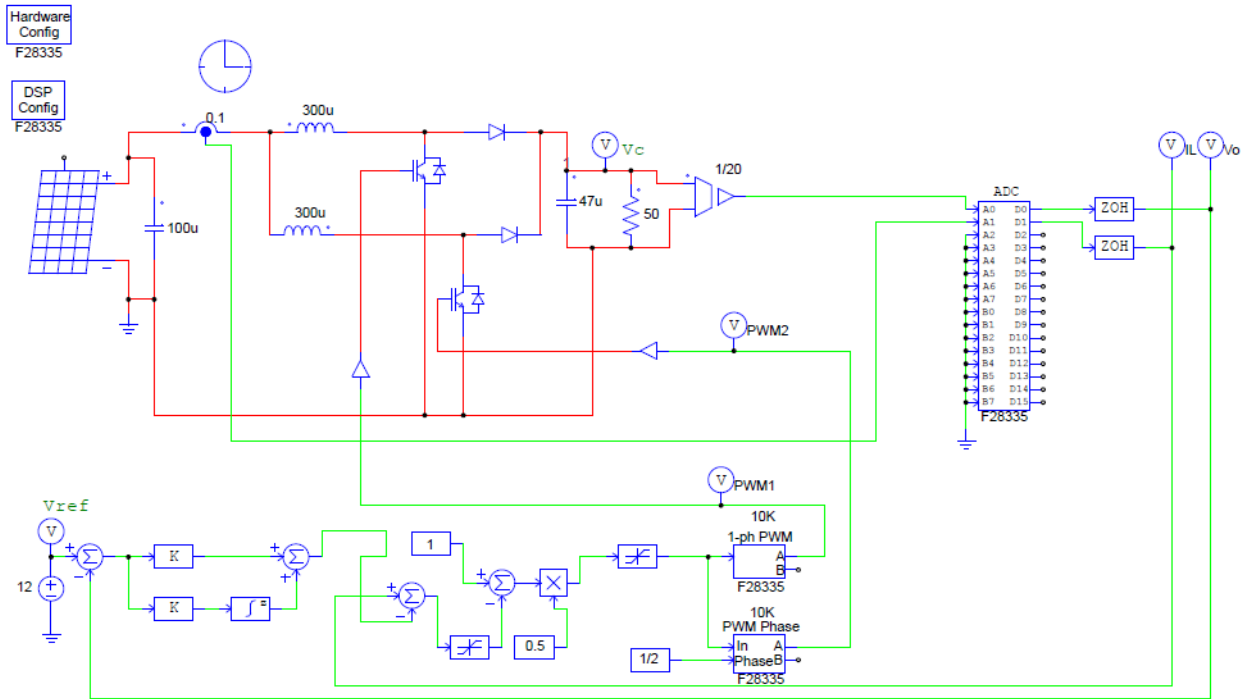The cascade PI-SMC is applied according to the control scheme displayed at Fig. 11.

Figure 11. PSIM discrete model of the control approach.

The sliding mode control theoretically uses the sign function, but it produces poor results in practice. Hence, it will be replaced by the saturation function to reduce switching and current ripples. The simulation results of the sliding mode control for the digital mode are shown in Figs. 12,13. A comparison with the PI-PI controller is also presented, along with a test for robustness against load perturbations. Since the switching frequency causes high harmonic components, a second-order low-pass filter with a 1KHz cutoff frequency is used to filter the current signal. The average values of the simulated discrete output voltage V_o and the input current of the converter i_L over a simulation time of 1 second are respectively 11.96 V and 0.423 A, indicating that the converter operates in continuous conduction mode (CCM). The simulation results demonstrate the effectiveness of the cascaded control scheme.
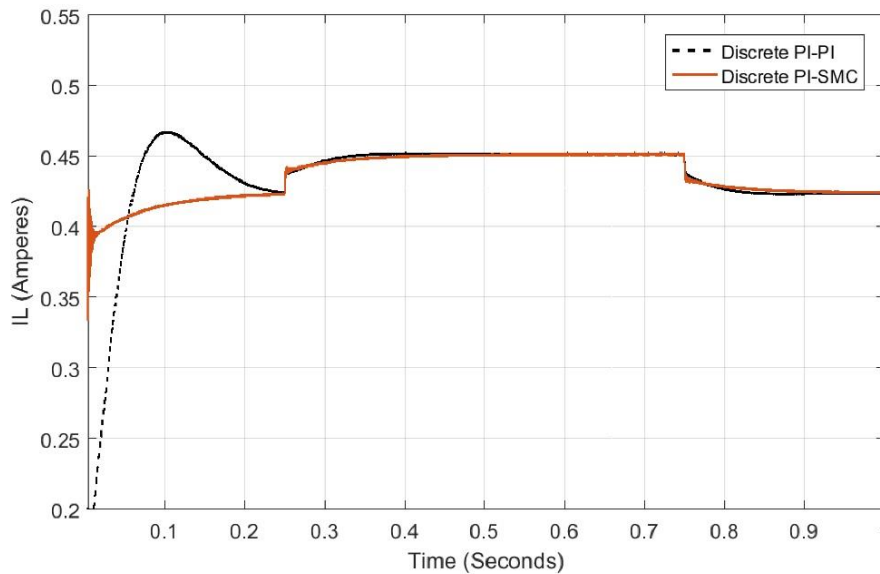

Figure 12. Total current in the input of the two-stage BC with 6% load perturbation between 0.25 s and 0.75 s.
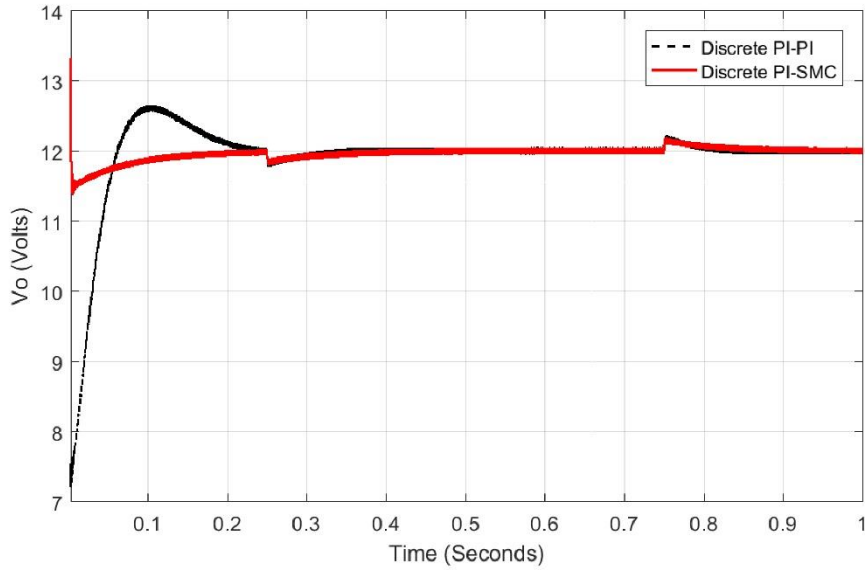
Figure 13. Output voltage simulation of the two-stage boost converter with 6% load perturbation.

4.3. Experimental Results and Discussion

The experimental results are resumed in Table 3. These values were measured by a voltmeter at the output of the solar panel and the converter. The error is static, it is calculated as $\left(\frac{V_O - 12}{12} \times 100\right)$.

Table 3. Experiments

Case test	Load (%)	$V_{in}(V)$	$V_O(V)$	Error (%)
Open loop 2IBC	100	6.89	14.54	21.16
Closed loop 2IBC	100	6.51	12.03	0.25
Closed loop 2IBC	104	5.92	12.03	0.25
Closed loop BC	100	6.36	11.94	0.5
Closed loop BC	104	6.32	11.94	0.5

Based on the general design scheme presented in Fig. 2, it is necessary to include a battery in practical applications to store the PV energy and avoid the influence of irradiation-dependent efficiency. However, this aspect is not within the scope of the experiments presented in this paper. The experimental results demonstrate the effectiveness of the closed-loop control strategy, with a static error of approximately 0.25%, even when the input voltage fluctuates randomly around 6 V_{dc}. Additionally, a load perturbation test was conducted, involving a 4% increase in charge caused by the activation of switch S_2 (Fig. 14), which shorts two 1 Ohm resistors. This perturbation had no effect on the output voltage, further validating the reliability of the control system.
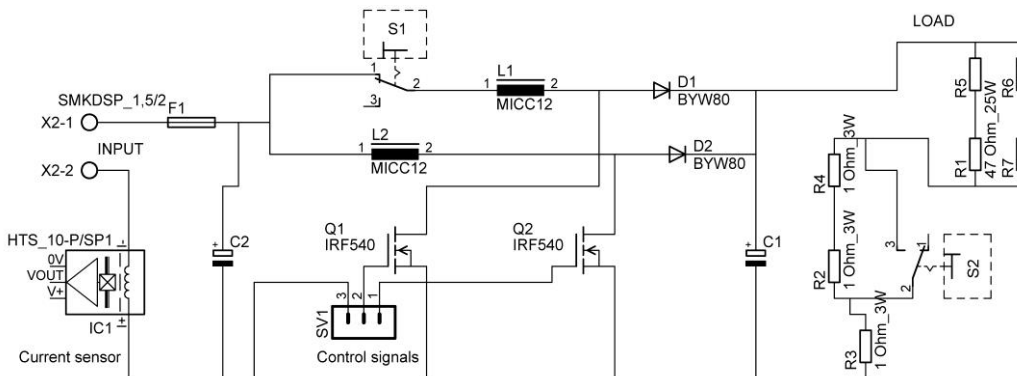

Figure 14. The electronic diagram of the power card.

When switch S_1 (refer to Fig. 14) is activated, the first stage goes offline and the circuit behaves like a conventional boost converter. Under this condition, the error observed was around 0.5%, and the effect of the same load perturbation was absent. This experiment validates the hardware redundancy of the power converter and demonstrates the possibility of overcoming a failure in one stage (which is typically caused by the transistor) by utilizing the second stage, which is designed to tolerate the delivered total current. Moreover, this step-up converter configuration is shown to be highly reliable, and the efficiency of the control scheme under test conditions is evident.

5. CONCLUSION AND PERSPECTIVE WORK

This work presents the design of a PV-based extra power supply for camping car applications, with a prototype assembly utilizing PI-SMC on a digital signal processor for control of the DC/DC power converter. The chattering phenomena caused by nonlinear sliding mode control is avoided in practice by using a saturation function instead of the sign function. The experiments are conducted with a static duty cycle of 0.5, and the linear transfer function of the two-stage boost converter is deduced to obtain the optimal parameters of the cascaded PI-PI controller. This controller is replaced in practice by PI-SMC for improved robustness against load perturbations and input voltage variations. Experimental tests of the closed-loop system reveal a very low level of static error even in the presence of load perturbations. The hardware redundancy of the power converter allows for passive fault-tolerant control with PI-SMC in the case of stage fault without reconfiguration of control parameters. The paper's main contribution is the demonstration of this control scheme, and testing of the converter with one operation stage shows reduced static error. While the design requires a battery and charger for reliable power supply, it is not constrained by temperature and irradiation perturbations. Future work may explore these areas further, and the authors have additional recent works in this area.

Acknowledgement

REFERENCES

[1] Lipu, M.S.H., Mamun, A.A., Ansari, S., Miah, M.S., Hasan, K., Meraj, S.T., Abdolrasol, M.G.M., Rahman, T., Maruf, M.H., Sarker, M.R., Aljanad, A., Tan, N.M.L. Battery Management, Key Technologies, Methods, Issues, and Future Trends of Electric Vehicles: A Pathway toward Achieving Sustainable Development Goals. *Batteries* 2022; *8*(9):119. https://doi.org/10.3390/batteries8090119.

[2] Xiong, S., Wenxian Y., Yingfu G., Kexiang W., Bo Q., Guanghui Z. A reliability study of electric vehicle battery from the perspective of power supply system. Journal of Power Sources, 2020;*451*(1);227805. https://doi.org/10.1016/j.jpowsour.2020.227805.

[3] Fan, Y., Yuanyuan, X., Yelin, D., Chris, Y. Impacts of battery degradation on state-level energy consumption and GHG emissions from electric vehicle operation in the United States. *Procedia CIRP* 2019; *80*: 530-535, ISSN 2212-8271, DOI:10.1016/j.procir.2018.12.010

[4] Barhate, S.S., Mudhalwadkar, R. Proton exchange membrane fuel cell fault and degradation detection using a coefficient of variance method. *Journal of Energy Systems* 2021; *5*(1), 20-34, DOI: 10.30521/jes.817879

[5] Paterson, S., Vijayaratnam, P., Perera C., Doig, G. Design and development of the Sunswift eVe solar vehicle: a record-breaking electric car. *Proceedings of the Institution of Mechanical Engineers, Part D: Journal of Automobile Engineering* 2016; *230*(14):1972-1986. DOI:10.1177/0954407016630153.

[6] Ben Said-Romdhane, M., Skander-Mustapha, S. A Review on Vehicle-Integrated Photovoltaic Panels. In: Motahhir, S., Eltamaly, A.M. (eds) Advanced Technologies for Solar Photovoltaics Energy Systems. Green Energy and Technology. Springer, Cham, 2021. https://doi.org/10.1007/978-3-030-64565-6_12.

[7] Cuce, E., Cuce, P.M., Bali, T. Impact of humidity on current parameters of solar cells. *Journal of Energy Systems* 2018; *2*(3): 84-96, DOI: 10.30521/jes.441643.

[8] Yılmaz Ekinci, S., Atun Sancaklı, S., Law, A.M., Walls, J.M. Performance and durability of thin film solar cells via testing the abrasion resistance of broadband anti-reflection coatings. *Journal of Energy Systems* 2022; *6*(1): 33-45, DOI: 10.30521/jes.952231

[9] Zaidi, A., Barambones, O., Charaabi, A., Zanzouri, N. Fault Tolerant Robust Passivity-Based Control Design for a Proton Exchange Membrane Fuel Cell Power Supply. *Journal of Energy Resources Technology* 2022; *144*(10):101304.

[10] Reshma Gopi, R., Sreejith, S. Converter topologies in photovoltaic applications: A review. *Renewable and Sustainable Energy Reviews* 2018; *94*: 1-14. DOI: 10.1016/j.rser.2018.05.047

[11] Luchetta, A., Manetti, S., Piccirilli, M.C., Alberto and al. Comparison of dcm operated pwm dc-dc converter modelling methods including the effects of parasitic components on duty ratio constraint. In: *IEEE 15th International Conference on Environment and Electrical Engineering* (EEEIC); 10-13 June 2015: IEEE; 766-771.

[12] Reatti, A., Corti, F., Tesi, A., Torlai A., Kazimierczuk, M.K. Effect of parasitic components on dynamic performance of power stages of DC-DC pwm buck and boost converters in ccm. In: *IEEE International Symposium on Circuits and Systems* (ISCAS); 26-29 May 2019: IEEE,1-5.

[13] Sheik Mohammed, S., Devaraj, D. Simulation of incremental conductance MPPT based two phase interleaved boost converter using MATLAB/simulink. In: *IEEE International Conference on Electrical, Computer and Communication Technologies* (ICECCT); 5-7 March 2015: IEEE. DOI: 10.1109/ICECCT.2015.7225987

[14] Swamy, H.M.M., Guruswamy, K.P., Singh, S.P. Design, Modeling and Analysis of Two Level Interleaved Boost Converter. In: International Conference on Machine Intelligence and Research Advancement; 21-23 December 2013: IEEE; 509-514. DOI :10.1109/icmira.2013.107

[15] Thounthong, P., Mungporn, P., Guilbert, D., Takorabet, N., pierfederici, S, Nahid-Mobaraked, B., Hu, Y., Bizon, N., Huangfu, Y., Kuman, P. Design and control of multiphase interleaved boost converters-based on differential flatness theory for PEM fuel cell multi-stack applications. *International Journal of Electrical Power and Energy Systems* 2021; *124*:106346. DOI:10.1016/j.ijepes.2020.106346

[16] Olmos-Lopez, A., Guerrero, G., Arau J., Aguilar C., Yris J. C. Passivity-based control for current sharing in PFC interleaved boost converters. In: Twenty-Sixth Annual IEEE Applied Power Electronics Conference and Exposition (APEC); 06-11 March 2011; IEEE, 475-480. DOI :10.1109/apec.2011.5744639

[17] Kamaraj, P.,Thamizharasu, T., Priya, M.V.,Voltage regulation of soft switched interleaved boost converter using fuzzy proportional integral controller. *Journal of Energy Systems* 2020, *4*(4), 145-160, DOI:10.30521/jes.762506.

[18] Charaabi, A., Barambones, O., Zaidi, A., Zanzouri, N. A Novel Two Stage Controller for a DC-DC Boost Converter to Harvest Maximum Energy from the PV Power Generation. *Actuators* 2020; *9*(2):29. DOI:10.3390/act9020029.

[19] Premchand, M., Gudey, S.K. Electric vehicle operation modes with reactive power support using SMC in distribution generation. *Journal of Energy Systems* 2020; *4*(3): 96-120, DOI: 10.30521/jes.731845.

[20] Saheb, S.S., Gudey, S.K. Robust fractional order sliding mode control for solar based DC AC inverter. *Journal of Energy Systems* 2020; *4*(4): 161-178, DOI: 10.30521/jes.737264.

[21] Charaabi, A., Zaidi, A., Zanzouri, N. Dual loop control of DC-DC boost converter-based cascade sliding mode control. In: International Conference on Green Energy Conversion Systems (GECS); 23-25 March 2017: IEEE, 1-6. DOI: 10.1109/GECS.2017.8066151

[22] Wu, C., Sehab, R., Akrad, A., Morel, C. Fault Diagnosis Methods and Fault Tolerant Control Strategies for the Electric Vehicle Powertrains. *Energies* 2022;*15*(13): 4840. https://doi.org/10.3390/en15134840

[23] Zenteno-Torres, J., Cieslak,J., Davila, J., Henry, D. Sliding Mode Control with Application to Fault-olerant Control: Assessment and Open Problems. *Automation* 2021; *2*: 1–30. DOI :10.3390/automation2010001

[24] Sri Revathi, B., Mahalingam, P., Gonzalez-Longatt, F. Interleaved high gain DC-DC converter for integrating solar PV source to DC bus. *Solar Energy* 2019; *188*: 924-934.

[25] Hafez, A.A., Hatata, A.Y., Alsubaihi, M.I., Alotaibi, R.M., Alqahtani, F.R., Alotaibi, S.O., Alhusayni, A.M., Alharbi, M.D. High Power Interleaved Boost Converter for Photovoltaic Applications. *Journal of Power and Energy Engineering* 2018; *6*(5):1-17.

[26] Jung, D.Y., Ji, Y.H., Park, S.H., Jung, Y.C., Won, C.Y. Interleaved Soft-Switching Boost Converter for Photovoltaic Power-Generation System. *IEEE Transactions on Power Electronics* 2011; *26*(4):1137-1145.

[27] Yang, F, Ruan, X, Wu G, and Ye Z. Discontinuous-current mode operation of a two-phase interleaved boost dc-dc converter with coupled inductor. *IEEE Transactions on Power Electronics* 2018; *33*(1):188-198.

[28] Balci, S., Sabanci, K. Performance analysis in a two-phase interleaved DC-DC boost converter with coupled inductors. International Journal of Applied Mathematics Electronics and Computers. 2022; *10*(4): 76-83.

[29] Jantharamin, N., Zhang, L. Analysis of Multiphase Interleaved Converter by using State-space Averaging Technique. In: ECTI-CON 6th international conference publications; 06-09 May 2009: IEEE, 288-291.

[30] Bougrine, M., Benmiloud, M., Benalia, A., Delaleau, E., Benbouzid, M. Load estimator-based hybrid controller design for two-interleaved boost converter dedicated to renewable energy and automotive applications. *ISA Transactions* 2016; *66*:425-436.

[31] Cisneros, R, Pirro, M., Bergna G., Ortega, R., Ippoliti, G., Molinas, M. Global tracking passivity-based PI control of bilinear systems: Application to the interleaved boost and modular multilevel converters. *Control Engineering Practice* 2015; *43*:109-119.

[32] Liangcai, X., Yigeng, H., Qian, L., Rui, M., Dongdong, Z., Qingchao, Z. Robust Control of a Interleaved Boost Converter Which Feeds a Constant Power Load for Electric Vehicles. In: IEEE Transportation Electrification Conference and Expo (ITEC); 19-21 June 2019: IEEE, DOI: 10.1109/ITEC.2019.8790527

[33] Chen, Z., Gao, W., Hu, J., Ye, X. Closed-Loop Analysis and Cascade Control of a Non-minimum Phase Boost Converter. *IEEE Transactions on Power Electronics* 2011; *26*(4):1237-1252.

[34] Utkin, V.I. Variable structure systems with sliding modes. *IEEE Transactions on Automatic Control* 1977; *22*: 211-222.

[35] Sira-Ramirez, H. Sliding mode control: The Delta sigma Modulation Approach. Springer International Publishing AG Switzerland 2015.

[36] Slotine, J-J E. Sliding controller design for non-linear systems. *International Journal of Control* 1948; *40*(2):421-434. DOI: 10.1080/00207178408933284